universe

MDPI

Article

Constraints on Lorentz Invariance Violation from Gamma-Ray Burst Rest-Frame Spectral Lags Using Profile Likelihood

Vyaas Ramakrishnan and Shantanu Desai *

Department of Physics, IIT Hyderabad, Kandi 502284, Telangana, India; vyaas3305@gmail.com
* Correspondence: shntn05@gmail.com

Abstract: We reanalyze the spectral lag data for 56 Gamma-Ray Bursts (GRBs) in the cosmological rest frame to search for Lorentz Invariance Violation (LIV) using frequentist inference. For this purpose, we use the technique of profile likelihood to deal with the nuisance parameters, corresponding to a constant time lag in the GRB rest frame and an unknown intrinsic scatter, while the parameter of interest is the energy scale for LIV (E_{QG}). With this method, we do not obtain a global minimum for χ^2 as a function of E_{QG} up to the Planck scale. Thus, we can obtain one-sided lower limits on E_{QG} in a seamless manner. Therefore, the 95% c.l. lower limits which we thus obtain on E_{QG} are then given by $E_{QG} \geq 2.07 \times 10^{14}$ GeV and $E_{QG} \geq 3.71 \times 10^{5}$ GeV, for linear and quadratic LIV, respectively.

Keywords: Gamma-Ray Bursts; Lorentz Invariance Violation; profile likelihood

1. Introduction

Spectral lags of Gamma-Ray Bursts (GRBs) have been widely used as a probe of Lorentz Invariance Violation (LIV) [1–3]. The spectral lag is defined as the time difference between the arrival of high-energy and low-energy photons and is considered to be positive if the high-energy photons precede the low-energy ones. In the case of LIV caused by an energy-dependent slowdown of the speed of light, one expects a turnover in the spectral lag data at higher energies.

Most of the searches for LIV using GRB spectral lags have been carried out using fixed-energy intervals in the observer frame. The first work to search for LIV using spectral lags between fixed rest-frame energy bands was the analysis in Wei and Wu [4] (W17, hereafter). This work considered a sample of 56 Swift-BAT detected GRBs, with spectral lags in the fixed rest-frame energy bands 100–150 keV and 200–250 keV [5]. Based on a Bayesian analysis, W17 obtained a robust lower limit on the LIV energy scale, $E_{QG} \geq 2.2 \times 10^{14}$ GeV at 95% credible intervals.

In the recent two decades, Bayesian statistics has become the industry standard for parameter inference in almost all areas of astrophysics and cosmology [6], including in searches for LIV. However, there has been a renaissance in the use of frequentist statistics in the field of cosmology, over the past 2–3 years, where the nuisance parameters were dispensed with using profile likelihood [7–11]. Some of the advantages and disadvantages of profile likelihood as compared to Bayesian analysis have been reviewed in the aforementioned works.

In this work, we redo the analysis in W17 using frequentist analysis, where we once again deal with nuisance parameters using profile likelihood. This manuscript is structured as follows. The analysis methodology is described in Section 2. Our results are discussed in Section 3, and we summarize our conclusions in Section 4.

check for updates

Academic Editors: Yongfeng Huang, He Gao, Liang Li and Jinjun Geng

Received: 29 March 2025
Revised: 20 May 2025
Accepted: 5 June 2025
Published: 6 June 2025

Citation: Ramakrishnan, V.; Desai, S. Constraints on Lorentz Invariance Violation from Gamma-Ray Burst Rest-Frame Spectral Lags Using Profile Likelihood. *Universe* **2025**, *11*, 183. https://doi.org/10.3390/universe11060183

Copyright: © 2025 by the authors. Licensee MDPI, Basel, Switzerland. This article is an open access article distributed under the terms and conditions of the Creative Commons Attribution (CC BY) license (https://creativecommons.org/licenses/by/4.0/).

2. Analysis Methodology

We briefly recap the equations used for the analysis of LIV following the same prescription and assumptions as in W17. The observed spectral time lag (Δt_{obs}) from a given GRB at a redshift z can be written down as

$$\frac{\Delta t_{obs}}{1+z} = a_{LIV}K + \langle b \rangle, \tag{1}$$

where $a_{LIV}K$ is given by the following expression for superluminal LIV [12] as follows:

$$a_{LIV}K = \frac{1+n}{2H_0}\frac{E_h^n - E_l^n}{(1+z)^n E_{QG,n}^n}\int_0^z \frac{(1+z')^n dz'}{\sqrt{\Omega_M(1+z')^3 + 1 - \Omega_M}}, \tag{2}$$

where n indicated the order of LIV and is equal to 1 and 2 for linear and quadratic LIV, respectively; Ω_M and H_0 are the cosmological parameters corresponding to the matter density and Hubble constant, respectively. We used the same values for the cosmological parameters as W17 (viz. $\Omega_M = 0.308$ and $H_0 = 67.8$ km/s/Mpc). The energies E_h and E_l correspond to the energies in the rest-frame bands, from which the spectral lags were obtained with $E_h > E_l$. The second term in Equation (1), namely $\langle b \rangle$, represents the average effect of intrinsic time lags (due to astrophysics), as discussed in W17. Although a large number of phenomenological models have been used to model the intrinsic spectral lag [1], here we model the astrophysical lag by a constant term similar to W17 for a straightforward comparison.

Similar to W17, we fit the observable $\frac{\Delta t_{obs}}{1+z}$ to Equation (1) using maximum likelihood estimation and by adding an additional intrinsic scatter (σ_{int}) to the observed uncertainties in the spectral lags

$$\mathcal{L}(E_{QG}, \sigma_{int}, \langle b \rangle) = \prod_{i=1}^{N} \frac{1}{\sqrt{\left(\frac{\sigma_i}{1+z}\right)^2 + \sigma_{int}^2}} \exp\left\{ -\frac{\left(\frac{\Delta t_{obs}}{1+z} - a_{LIV}K - \langle b \rangle\right)^2}{2\left(\sigma_{int}^2 + \left(\frac{\sigma_i}{1+z}\right)^2\right)} \right\}, \tag{3}$$

where σ_i is the uncertainty in Δt_{obs}, and σ_{int} is the unknown intrinsic scatter, which we fit for. Therefore, our regression problem contains three unknown parameters: E_{QG}, $\langle b \rangle$, and σ_{int}. In this problem, $\langle b \rangle$ and σ_{int} represent the nuisance parameters, which we account for using profile likelihood to obtain the likelihood distribution as a function of E_{QG}:

$$\mathcal{L}(E_{QG}) = \max_{\sigma_{int}, \langle b \rangle} \mathcal{L}(E_{QG}, \sigma_{int}, \langle b \rangle) \tag{4}$$

For ease of computation, instead of maximizing Equation (4), we construct χ^2 which is defined as

$$\chi^2 \equiv -2 \ln L(E_{QG}, \sigma_{int}, \langle b \rangle) \tag{5}$$

We then minimize χ^2 defined in Equation (5) over σ_{int} and $\langle b \rangle$ for a fixed value of E_{QG}. We then obtain frequentist confidence intervals (or upper limits) on E_{QG} from $\Delta\chi^2(E_{QG}) = \chi^2(E_{QG}) - \chi^2_{min}$, where χ^2_{min} is the global minimum for χ^2 over all values of E_{QG}. For this purpose, we use Wilks' theorem, which states that $\Delta\chi^2$ follows a χ^2 distribution for one degree of freedom [13].

3. Results

We now apply the methodology in the previous section to the spectral lag data of 56 Swift-BAT detected GRBs, consisting of both short and long GRBs collated in Bernardini et al. [5], where the spectral lags were calculated in fixed rest-frame energy bands of

100–150 keV and 200–250 keV. This dataset consists of GRBs with redshifts ranging from 0.35 (GRB 061021) to 5.47 (GRB 060927), having a mean redshift of 1.73. The energy gap between the midpoints of the successive rest-frame energy intervals is fixed at 100 keV. The uncertainties in the spectral delay are calculated by averaging the left and right uncertainties provided in the aforementioned work. The full details of the 56 GRBs used for the analysis, such as the GRB name, redshift, observed spectral lags, and their uncertainties, can be found in Table 1 of Bernardini et al. [5].

To evaluate profile likelihood, we construct a logarithmically spaced grid for E_{QG} from 10^5 GeV to 10^{19} GeV for linear and quadratic models of LIV. The upper bound of 10^{19} GeV corresponds to the Planck scale. For each value of E_{QG}, we calculate the minimum value of $\chi^2(E_{QG})$ by minimizing over σ_{int} and $\langle b \rangle$. This minimization was carried out using the `scipy.optimize.fmin` function, which uses the Nelder–Mead simplex algorithm [14]. We also cross-checked this result with other minimization algorithms available in `scipy` and found that the results do not change.

We find that χ^2 does not achieve global minima below the Planck scale (E_{pl}). We then plot the curves of $\Delta\chi^2$ as a function of E_{QG} for the linear and quadratic models of LIV, where $\Delta\chi^2 = \chi^2(E_{QG}) - \chi^2(E_{pl})$. These $\Delta\chi^2$ curves can found in Figures 1 and 2, for linear and quadratic models of LIV, respectively. Since we do not obtain global minima below the Planck scale, we can set one-sided 95.4% confidence level (c.l.) lower limits, by finding the x-intercept for which $\Delta\chi^2 = 4$. For brevity, we denote 95.4% c.l. as 95% c.l. These 95% c.l. lower limits are given by $E_{QG} \geq 2.07 \times 10^{14}$ GeV and $E_{QG} \geq 3.71 \times 10^5$ GeV, for linear and quadratic LIV, respectively. Therefore, we can set lower limits on the energy scale of LIV in a seamless manner, since we do not obtain a global minimum. Since our main aim was to compare our results to W17, we used the same cosmological parameters as those in W17. When we vary the cosmological parameters and use the latest values from PDG, viz. $H_0 = 67.4$ km/s and $\Omega_m = 0.315$, we do not find qualitative differences in the shape of χ^2 as a function of E_{QG}. The new 95% lower limits on E_{QG} change to $E_{QG} \geq 2.08 \times 10^{14}$ GeV and $E_{QG} \geq 3.71 \times 10^5$ GeV, for linear and quadratic LIV, respectively. Therefore, the variation in the lower limit on E_{QG} is negligible upon choosing the PDG cosmological parameters.

In order to judge the efficacy of the fit, similar to W17, we calculate the χ^2_{fit} based on the residuals between the data and best-fit model, as follows:

$$\chi^2_{fit} = \sum_i \frac{\left(\frac{\Delta t_i}{1+z_i} - a_{\rm LIV} K_i - \langle b \rangle\right)^2}{\sigma^2_{\rm int} + \left(\frac{\sigma_i}{1+z_i}\right)^2} \,. \tag{6}$$

Note that χ^2_{fit} is used to ascertain the quality of the fit and is different from χ^2 defined in Equation (5). We evaluated χ^2_{fit} and χ^2_{fit}/DOF for values of E_{QG} at both the Planck scale and the 95% cl. lower limit on E_{QG} for both the LIV models. Here, DOF refers to the degrees of freedom, being equal to the difference between the total number of data points and the number of free parameters (three). These values can be found in Table 1. We also show the best-fit values of $\langle b \rangle$ and σ_{int} in this table. We find that the best-fit values of $\langle b \rangle$ and σ_{int} are consistent within the 68% credible regions for the marginalized posteriors obtained in W17 (for linear LIV). The reduced χ^2_{fit} is close to one for both models, although it includes an intrinsic scatter of about 2%. In Appendix A, we compare the results of frequentist and Bayesian inference for bootstrapped version of the data where the uncertainties in the spectral lags are randomly swapped.

Table 1. Best-fit model parameters, $\langle b \rangle$ and σ_{int}, corresponding to both linear and quadratic LIV models, evaluated at their respective 95% confidence lower limits of E_{QG}. The standard frequentist goodness-of-fit metric, χ^2_{fit}/DOF (refer to Equation (6)), is also reported at both the 95% c.l. lower limit for E_{QG} and at the Planck scale. Here, DOF refers to the degrees of freedom, being equal to the difference between the total number of data points and the number of free parameters.

	Linear LIV $\mathbf{n = 1}$		**Quadratic LIV** $\mathbf{n = 2}$	
$\langle b \rangle$	-0.035		-0.011	
σ_{int}	0.023		0.023	
E_{QG} (GeV)	2.07×10^{14}		3.71×10^{5}	
	$\mathbf{E_{QG}}$	$\mathbf{E_{pl}}$	$\mathbf{E_{QG}}$	$\mathbf{E_{pl}}$
χ^2_{fit}/DOF	52.88/54	53.91/54	52.46/54	53.95/54

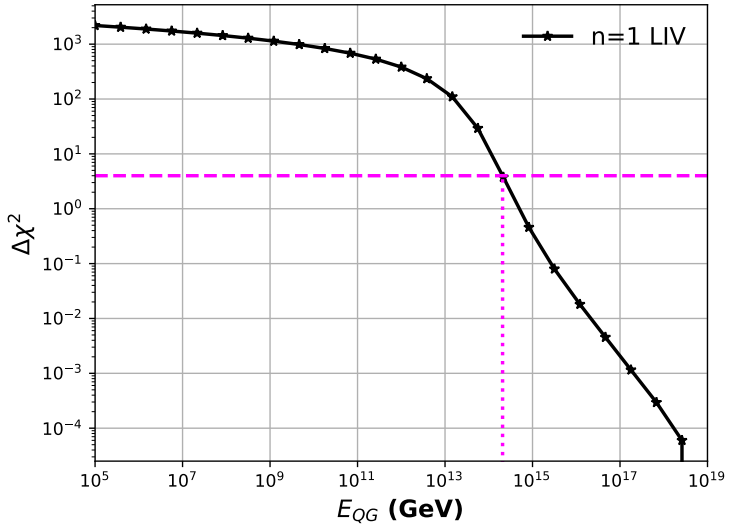


Figure 1. $\Delta\chi^2$, defined as $(\chi^2 - \chi^2_{E_{pl}})$, plotted against E_{QG} for a linearly dependent LIV, corresponding to $n = 1$, in Equation (2). The horizontal magenta dashed line represents $\Delta\chi^2 = 4$, and the vertical magenta dashed line provides us the x-intercept, the 95% confidence level lower limit for $E_{QG} = 2.07 \times 10^{14}$ GeV.

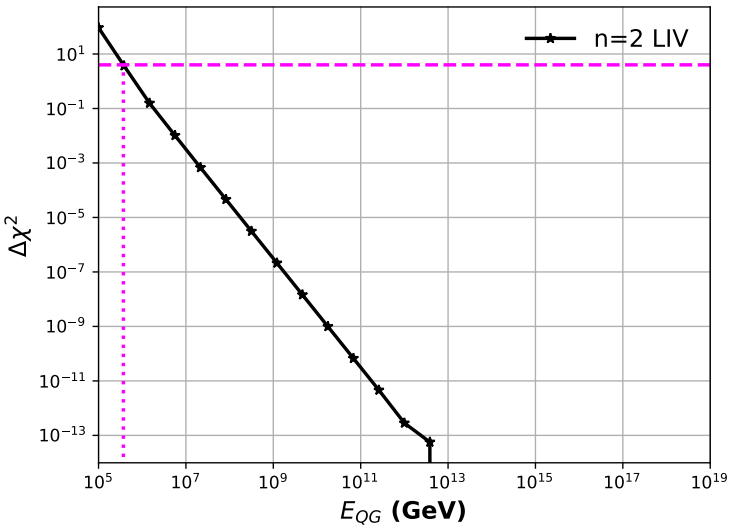


Figure 2. $\Delta\chi^2$, defined as $(\chi^2 - \chi^2_{E_{pl}})$, plotted against E_{QG} for a quadratically dependent LIV, corresponding to $n = 2$, in Equation (2). The horizontal magenta dashed line represents $\Delta\chi^2 = 4$, and the vertical magenta dashed line provides us the x-intercept, the 95% confidence level lower limit for $E_{QG} = 3.71 \times 10^5$ GeV.

4. Conclusions

In this work, we have reanalyzed the data for spectral lags of 56 GRBs between two fixed energy bands in the rest frame, in order to search for LIV using frequentist inference. For this analysis, we use profile likelihood to deal with the astrophysical nuisance parameters, and we set a constraint on the energy scale of LIV for both linear and quadratic models.

We parametrize the rest-frame spectral lags as a sum of a constant intrinsic lag and LIV-induced time lag. Similarly to W17, we use a Gaussian likelihood and also incorporate another free parameter for the intrinsic scatter, which is added in quadrature to the observed uncertainties in the spectral lags. Therefore, our regression model consists of two nuisance parameters and one physically interesting parameter, viz. the energy scale for LIV.

We find that after dealing with nuisance parameters using profile likelihood, we do not find a global minimum for χ^2 as a function of E_{QG} below the Planck energy scale. These plots for $\Delta\chi^2$ as a function of LIV for both the linear and quadratic models of LIV are shown in Figure 1 and Figure 2, respectively. Therefore, we can set one-sided lower limits at any confidence levels from the X-intercept of the $\Delta\chi^2$ curves. These 95% confidence level lower limits obtained from $\Delta\chi^2 = 4$ are given by $E_{QG} \geq 2.07 \times 10^{14}$ GeV and $E_{QG} \geq 3.71 \times 10^5$ GeV, for linear and quadratic LIV, respectively. Our lower limit for linear LIV is comparable to the value obtained in W17 (2.2×10^{14} GeV). The best-fit values for the two nuisance parameters evaluated at two different energies (Planck scale and 95% c.l. lower limit value) can be found in Table 1.

Therefore, we have shown that the profile likelihood method provides a viable alternative in dealing with nuisance parameters, which is complementary to the widely used Bayesian inference technique, and for our example, allows us to seamlessly infer the lower limits in an automated manner. In the spirit of open science, we have made our analysis codes publicly available, and they can be found on Github (https://github.com/vyaas3305/liv-PL-restframe, accessed on 1 March 2025).

Author Contributions: Conceptualization, V.R. and S.D.; Writing—review & editing, V.R. All authors have read and agreed to the published version of the manuscript.

Funding: This research received no external funding.

Data Availability Statement: The original data presented in the study are openly available in https://github.com/vyaas3305/liv-PL-restframe.

Conflicts of Interest: The authors declare no conflicts of interest.

Appendix A

In order to ensure that the differences in our results between frequentist and Bayesian analysis are not due to statistical fluctuations, we redo the analysis by completing random swapping of parameter uncertainties among the 56 GRBs, in order to check the robustness of our results. To avoid altering the redshifts and the spectral lags of the observed GRBs, we only swap the uncertainties in the spectral lags amongst the GRBs, and then repeat both Bayesian and frequentist analyses. All the other parameters therefore remain the same. For Bayesian analysis, we use the same likelihood as in Equation (3) and uniform priors on $\log(E_{QG})$, b, and σ_{int}, given by $\mathcal{U}$ (1,19), $\mathcal{U}$ (−1.0,1.0), and $\mathcal{U}$ (0,1.0), respectively.

The results of the profile likelihood analysis can be found in Figures A1 and A2 for linear and quadratic LIV, respectively. We find that the $\Delta\chi^2$ plot as a function of E_{QG} does not show a global minimum for the linear model of LIV, similar to before. The 95% c.l. lower limit on E_{QG} using these shuffled uncertainties is given by $E_{QG} \geq 3.1 \times 10^{14}$ GeV. For the quadratic LIV case, although we obtain a global minimum below the Planck scale,

we find that $\Delta\chi^2$ asymptotes towards a constant value of 1.4 above the global minima. Therefore, similar to before, we can only set one-sided lower limits on E_{QG} at 95% c.l., since $\Delta\chi^2$ does not exceed the value of 4.0 after its minimum. Therefore, the lower limit on E_{QG} at 95% c.l. is given by $E_{QG} \geq 1.8 \times 10^5$ GeV. Therefore, these frequentist limits using the shuffled data are of the same order of magnitude as those obtained using the original data.

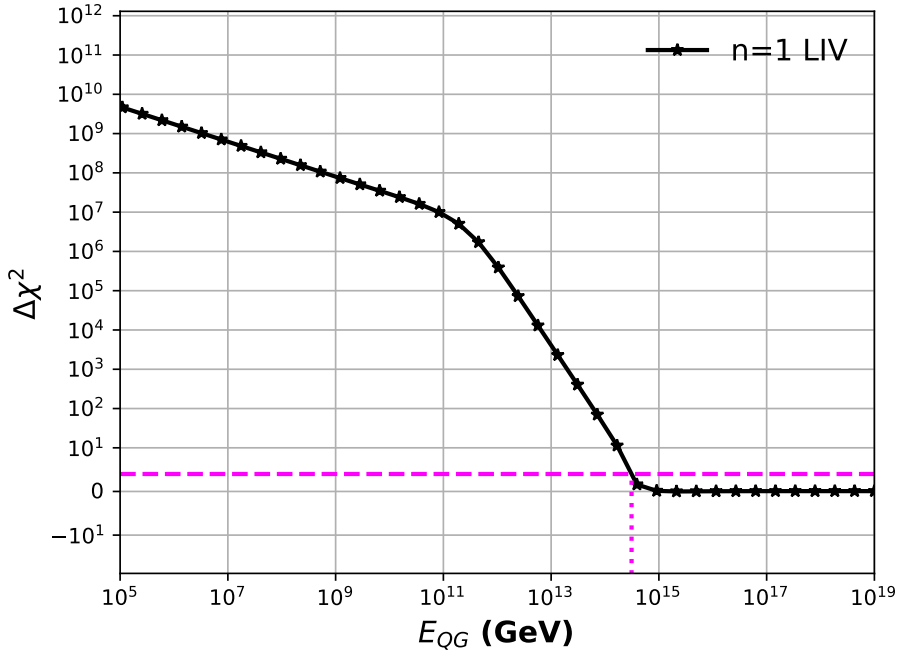


Figure A1. $\Delta\chi^2$, defined as $(\chi^2 - \chi^2_{E_{pl}})$, plotted against E_{QG} for a linearly dependent LIV, corresponding to $n = 1$, in Equation (2), after shuffling the uncertainties in the spectral lags among the GRBs. The horizontal magenta dashed line represents $\Delta\chi^2 = 4$, and the vertical magenta dashed line provides us the x-intercept, the 95% confidence level lower limit for $E_{QG} = 3.1 \times 10^{14}$ GeV.

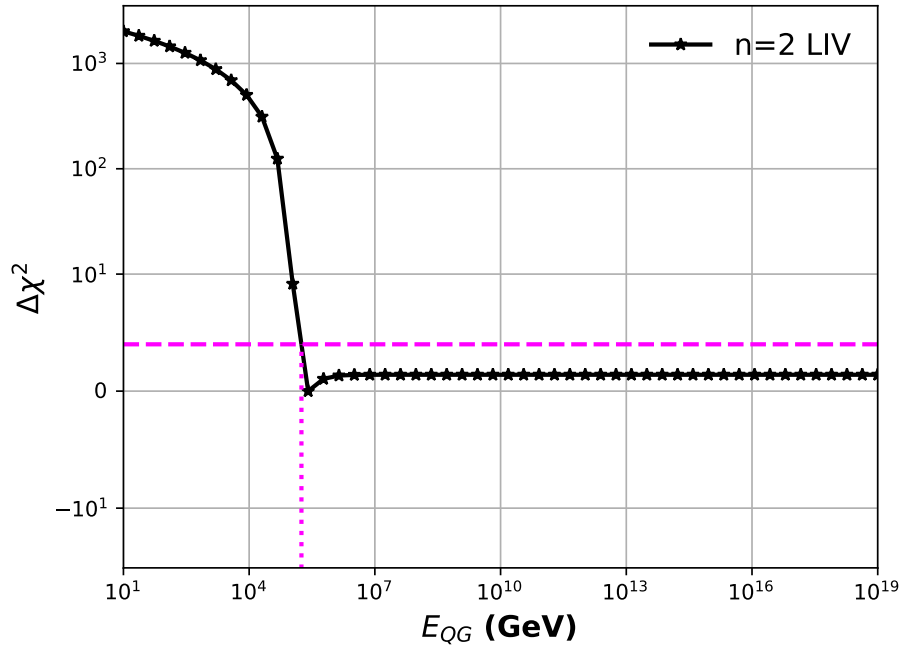


Figure A2. $\Delta\chi^2$, defined as $(\chi^2 - \chi^2_{E_{pl}})$, plotted against E_{QG} for a quadratically dependent LIV, corresponding to $n = 2$, in Equation (2), after shuffling the uncertainties in the spectral lags among the GRBs. The horizontal magenta dashed line represents $\Delta\chi^2 = 4$, and the vertical magenta dashed line provides us the x-intercept, the 95% confidence level lower limit for $E_{QG} = 1.8 \times 10^5$ GeV.

The corresponding Bayesian credible intervals for all the three free parameters can be found in Figures A3 and A4, for linear and quadratic LIV models, respectively. We find that we do not obtain bounded marginalized 95% credible intervals for E_{QG} for both linear as well as quadratic LIV models. This behavior is qualitatively similar to that seen for frequentist analysis. Therefore, we can only set one-sided Bayesian lower limits. These lower limits at 95% credible intervals are given by $E_{QG} \geq 3.1 \times 10^{14}$ GeV and $E_{QG} \geq 1.8 \times 10^{5}$ GeV for linear and quadratic LIV, respectively. These limits marginally differ from the corresponding frequentist lower limits, despite being of the same order of magnitude.

Therefore, we find that once we shuffle the uncertainties in the spectral lags, although we do not obtain closed intervals for E_{QG} at 95% confidence/credible intervals using both frequentist and Bayesian analyses, the limits are marginally different. However, we note these results are obtained using only one realization of the bootstrapped data.

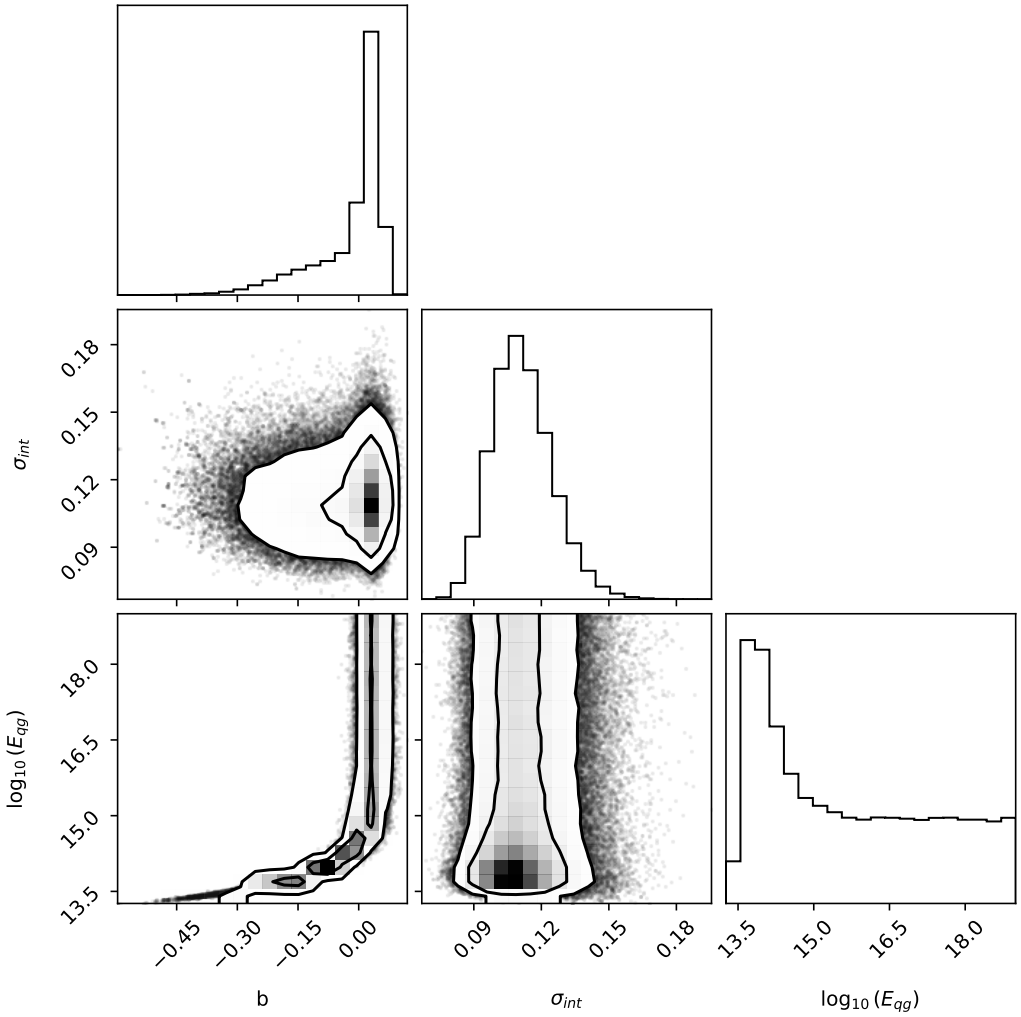


Figure A3. The marginalized contours for E_{QG}, b and σ_{int} at 68% and 95% credible intervals for a linear model of LIV, corresponding to $n = 1$, in Equation (2). The corresponding 95% lower limit for E_{QG} is given by $E_{QG} = 3.66 \times 10^{13}$ GeV.

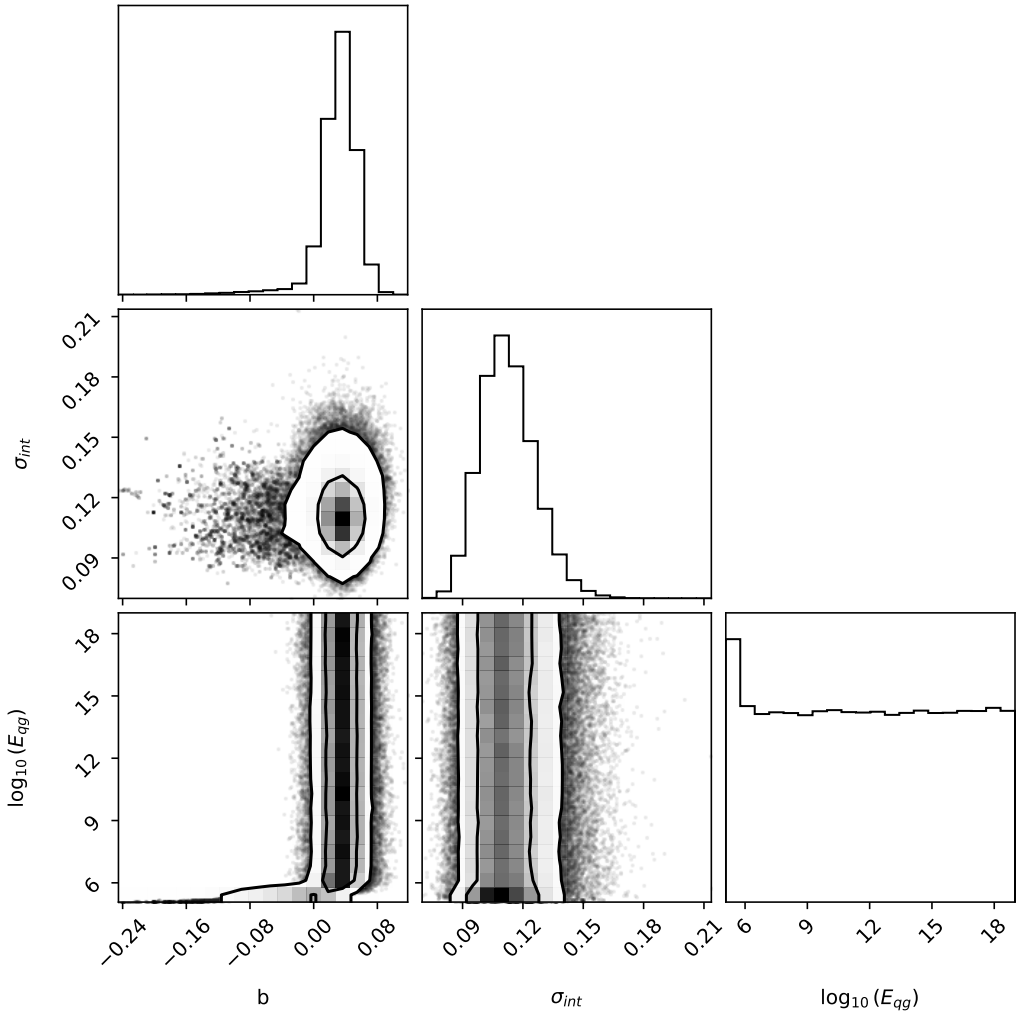


Figure A4. The marginalized contours for E_{QG}, b and σ_{int} at 68% and 95% credible intervals for a quadratic model of LIV, corresponding to $n = 2$, in Equation (2) The corresponding 95% lower limit for E_{QG} is given by $E_{QG} = 2.01 \times 10^5$ GeV.

References

1. Desai, S. Astrophysical and Cosmological Searches for Lorentz Invariance Violation. In *Recent Progress on Gravity Tests. Challenges and Future Perspectives*; Bambi, C., Cárdenas-Avendaño, A., Eds.; Springer: Berlin/Heidelberg, Germany, 2024; pp. 433–463. [CrossRef]
2. Yu, Y.W.; Gao, H.; Wang, F.Y.; Zhang, B.B. Gamma-Ray Bursts. In *Handbook of X-Ray and Gamma-Ray Astrophysics*; Bambi, C., Santangelo, A., Eds.; Springer: Berlin/Heidelberg, Germany, 2022; p. 31. [CrossRef]
3. Wei, J.J.; Wu, X.F. Tests of Lorentz Invariance. In *Handbook of X-Ray and Gamma-Ray Astrophysics*; Bambi, C., Santangelo, A., Eds.; Springer: Berlin/Heidelberg, Germany, 2022; p. 82. [CrossRef]
4. Wei, J.J.; Wu, X.F. A Further Test of Lorentz Violation from the Rest-frame Spectral Lags of Gamma-Ray Bursts. *Astrophys. J.* **2017**, *851*, 127. [CrossRef]
5. Bernardini, M.G.; Ghirlanda, G.; Campana, S.; Covino, S.; Salvaterra, R.; Atteia, J.L.; Burlon, D.; Calderone, G.; D'Avanzo, P.; D'Elia, V.; et al. Comparing the spectral lag of short and long gamma-ray bursts and its relation with the luminosity. *Mon. Not. R. Astron. Soc.* **2015**, *446*, 1129–1138. [CrossRef]
6. Trotta, R. Bayesian Methods in Cosmology. *arXiv* **2017**, arXiv:1701.01467.
7. Herold, L.; Ferreira, E.G.M.; Komatsu, E. New Constraint on Early Dark Energy from Planck and BOSS Data Using the Profile Likelihood. *Astrophys. J. Lett.* **2022**, *929*, L16. [CrossRef]
8. Campeti, P.; Komatsu, E. New Constraint on the Tensor-to-scalar Ratio from the Planck and BICEP/Keck Array Data Using the Profile Likelihood. *Astrophys. J.* **2022**, *941*, 110. [CrossRef]
9. Colgáin, E.Ó.; Pourojaghi, S.; Sheikh-Jabbari, M.M. Implications of DES 5YR SNe Dataset for ΛCDM. *arXiv* **2024**, arXiv:2406.06389. [CrossRef]

10. Karwal, T.; Patel, Y.; Bartlett, A.; Poulin, V.; Smith, T.L.; Pfeffer, D.N. Procoli: Profiles of cosmological likelihoods. *arXiv* **2024**, arXiv:2401.14225. [CrossRef]
11. Herold, L.; Ferreira, E.G.M.; Heinrich, L. Profile likelihoods in cosmology: When, why, and how illustrated with ΛCDM, massive neutrinos, and dark energy. *Phys. Rev. D.* **2025**, *111*, 083504. [CrossRef]
12. Jacob, U.; Piran, T. Lorentz-violation-induced arrival delays of cosmological particles. *J. Cosmol. Astropart. Phys.* **2008**, *1*, 031. [CrossRef]
13. Wilks, S.S. The large-sample distribution of the likelihood ratio for testing composite hypotheses. *Ann. Math. Stat.* **1938**, *9*, 60–62. [CrossRef]
14. Press, W.H.; Teukolsky, S.A.; Vetterling, W.T.; Flannery, B.P. *Numerical Recipes in FORTRAN: The Art of Scientific Computing*; Cambridge University Press: Cambridge, UK, 1992.

Disclaimer/Publisher's Note: The statements, opinions and data contained in all publications are solely those of the individual author(s) and contributor(s) and not of MDPI and/or the editor(s). MDPI and/or the editor(s) disclaim responsibility for any injury to people or property resulting from any ideas, methods, instructions or products referred to in the content.